Coal Adsorbents from Man-Made Waste to Reduce the Emission of Pharmaceutical Substances into the Environment

Kamoliddin Shadmanov[1], Abdusalom Umarov[2], Elena Mirzaeva[3], Dilnoza Turdiyeva[4], Iroda Abdurakhmanova[4], Shakhnoza Jalalova[5] and Sarvar Aliev[6]

[1]*Pharmaceutical Institute of Education and Research, 100100 Tashkent, Uzbekistan*
[2]*University of Tashkent for Applied Sciences, Gavhar Str. 1, 100149 Tashkent, Uzbekistan*
[3]*Branch of the National Research Technological University "MISIS" in Almalyk, 110100 Almalyk, Uzbekistan*
[4]*Mirzo Ulugbek National University of Uzbekistan, 100174 Tashkent, Uzbekistan*
[5]*Uzbek Scientific Research Chemical and Pharmaceutical Institute named after A. S. Sultanov, 100100 Tashkent, Uzbekistan*
[6]*Tashkent Medical Academy, 100109 Tashkent, Uzbekistan*
sarvaraliev1984@gmail.com, shodman@mail.ru, rektor@utas.uz, mirzaevaelena92@gmail.com, turdievadilnoza34@gmail.com, irodchka@mail.ru, shakhnoz65@mail.ru

Keywords: Adsorbents, Waste Processing, Alumina Waste, Pharmaceutical Pollutants.

Abstract: Preservation of the environment and resources has gained momentous proportions nowadays due to increase in the population, growth in industrial activities as well as enhanced production of hazardous waste thereof. One of the greatest environmental challenges is the development of an environmentally friendly, cutting-edge technology to prevent the release of pharmaceutical products into the environment via gaseous and liquid effluents from this industry. Households effluent often comprises high concentrations of drugs and their metabolites that are not completely converted in developing organisms. The objective of this research was to prepare coal adsorbents from byproducts of canning, cotton and oil-refining industries, characterize them by methods of physicochemical analysis and test their cleaning properties for pharmaceutical agent pollutants. Thermogravimetric analysis and infrared spectroscopy were used to investigate the production of activated carbons from plant waste substances. Removal percentages of pharmaceuticals and volatile organic compounds model mixtures were evaluated. Chemical modified peach seed shell carbonizate was used for obtaining activated carbon with developed mesoporous structure, the specific surface area of 835 m^2/g and a methylene blue sorption capacity of 186 mg/g; at that, adsorption layer from this carbon guaranteed not less than 97% uptake of acetone and metylchloride and up to 90% for methanol and toluene. Waste water treatment decreased COD by 50% or more to meet the discharge code.

1 INTRODUCTION

With the rapid development of the pharmaceutical industry, substantial amounts of pollution have been released into the environment, not only from drug manufacturing but also from toxic substances infiltrating sewage networks, landfills, and animal waste among others depending on their life cycle [1], [2]. Municipality wastewater treatment plants are considered as hot spots for pharmaceuticals, and medicinal, over-the-counter compounds [3]. Antibiotics, a widely used drug in human veterinary practice [4] have been detected in wastewater treatment plants and surface waters [5], [6]. Toxic volatile compounds from a variety of chemical classes: hydrocarbons, alcohols, acids, chlorinated compounds and others needing purification are released into the environment during the cycle process of synthesis-extraction-recrystallization [7]. Activated carbon adsorption [8]-[10] and coagulation [11], [12] still serve as traditional methods of wastewater treatment. Neutralisation of certain pollutants has been widely propagated through application of specific enzymes and non-pathogenic microorganisms. Recent developments are also underway, including phenol adsorption by aluminum oxide nanoparticles [13], photodegradation and photocatalysis together with analysis of selected water pollutants [14]. Electrochemical oxidation of recalcitrant organic

pollutants was investigated [15]-[21]. In some cases, neutralizing agents are preferred. For large volumes of flue gas containing insoluble constituents, a conventional activated-carbon slurry can be sprayed onto the gas stream to effectively adsorb the contaminants, thereby allowing valuable solvents to be recovered and re-enter production cycles.

The lack of high-quality natural coals and large volume of diverse waste products from woodworking [22] and agricultural businesses [23]-[25], require reasonable utilization as a source for active carbon production. In this investigation, coal adsorbents were prepared from shells of peach and apricot seeds, husk of seed and cotton stems (guza-pai). Regeneration of spent aluminum oxide adsorbents provided material suitable for use in the preparation of fresh adsorbents and coagulants. The physicochemical properties of the resulting adsorbents were characterized, and the prepared adsorbents were tested to absorb pharmaceutical products emitted into water.

2 MATERIALS AND METHODS

2.1 Conditions for Obtaining Adsorbents and Coagulants

Coal adsorbents were produced from waste materials of the canning industry (apricot seed shells, AU-A; peach seed shells, AU-P) and the cotton industry (cottonseed husks, AU-HS; cotton stalk residues, AU-GP) using a technology similar to that described by Ismailova et al. [26], but conducted under stationary conditions. Carbonization was performed in a heated steel reactor with continuous removal of pyrolysis products, following the methodology reported by Dzhalalova et al. [27].

Plant-based waste materials were crushed to a particle size of 0.2-0.4 mm and subjected to carbonization under a nitrogen atmosphere, alkaline modification, and steam activation. The optimal conditions for producing AU-A and AU-P adsorbents were carbonization at a heating rate of 6-8 °C·min^{-1} to 710 °C with a holding time of 60-65 min, followed by activation at 780-800 °C using a H_2O/carbonizate ratio of 5:1 for 70 min, resulting in a burnout degree of 35-40%. For AU-HS and AU-GP adsorbents, optimal conditions included carbonization at 7-9 °C·min^{-1} to 720 °C for 80-90 min and activation at 800 °C with a H_2O/carbonizate ratio of 4.5:1 for 50 min.

Chemical modification of dried plant waste and carbonized materials was carried out by impregnation with aqueous solutions of NaOH, Na_2CO_3, $NaHCO_3$, or KOH. The applied modifier is indicated in parentheses following the adsorbent code.

Granular aluminum oxide and combined coagulants were synthesized from spent adsorbents originating from a naphtha catalytic reforming unit, including deactivated Axsorb AA and Uz-AD-1 used for purification of chlorine-containing gases [28]. Water leaching of spent granules extracted sodium, aluminum, and iron chlorides. After evaporation, NaCl crystals were separated, and the remaining solution exhibited coagulating properties due to the presence of $AlCl_3 \cdot 6H_2O$. To enhance coagulation efficiency, aluminum sulfate solution obtained by dissolving washed waste adsorbents in 60% sulfuric acid was added, yielding coagulant K-1. Coagulant K-2 additionally contained $FeCl_3$.

Aluminum hydroxide was obtained by adding concentrated NH_4OH to the sulfuric acid solution of Uz-AD-1 while maintaining pH 7.6-7.8 and a temperature of 20-23 °C. The resulting AlOOH precipitate was extruded with polyvinyl alcohol as a pore-forming plasticizer, dried, and calcined at 550 °C to produce sample OA-1. Modified OA-1 granules were impregnated with alkaline solutions and calcined at 530-560 °C.

2.2 Research Methods

The mechanical strength of irregular activated carbon particles was assessed by abrasion resistance in a rotating three-chamber drum using a PIG-2 device. The amount of dust and fines generated after 15 min of rotation was measured. The mechanical strength of cylindrical OA-1 granules (4 mm diameter) was determined by end-face crushing tests and expressed in kg per granule.

Textural properties, including surface area and pore size distribution, were determined by mercury porosimetry (Carlo Erba) at pressures up to 200 MPa. Chemical composition at various preparation and testing stages was analyzed using a Hitachi B-8000 atomic emission spectrometer and scanning electron microscopy with energy-dispersive X-ray spectroscopy (SEM-EDX). Phase composition was determined by X-ray diffraction (Empyrean diffractometer, CuKα radiation, 30 kV, 20 mA).

Thermal analysis was performed using a HESON HS-TGA-103 derivatograph. Differential thermal analysis (DTA) and thermogravimetric (TG) curves

were recorded under identical conditions. Infrared spectroscopy was conducted using MIRacle 10 and Nicolet S50 FTIR spectrometers in the range of 4000-600 cm^{-1}. Surface functional groups were quantified by the Boehm titration method [29], [30].

Adsorption of methylene blue and purification efficiency of model wastewater were evaluated photometrically using a V-5000 spectrometer. Dynamic adsorption experiments were carried out in a column (diameter 1.5 cm, bed height 80 cm) at a flow rate of 140-142 $mL \cdot h^{-1}$. Removal of pharmaceutical compounds was assessed by changes in chemical oxygen demand (COD) using the dichromate method. Gas-phase adsorption experiments were performed using a Sgom-5 chromatograph equipped with flame ionization and thermal conductivity detectors.

2.3 Data Processing

All experimental results represent average values from three independent measurements. Standard deviations were calculated accordingly. The relative error in determining mechanical strength was 1-2%, while ash content determination accuracy ranged from 0.2 to 0.6%. Turbidity detection limits were 0.2 $mg \cdot L^{-1}$. Reproducibility of surface functional group measurements ranged from 85 to 90%. COD determination accuracy was 94-98% of the theoretical oxygen demand.

XRD patterns were interpreted using the International Centre for Diffraction Data (ICDD, 2019). IR spectra were analyzed based on characteristic absorption frequencies reported in the literature [31]-[33].

3 RESULTS

3.1 Physical and Chemical Characteristics

Elemental analysis of dried plant-based raw materials (random-point measurements) showed that cotton-industry wastes contained, on average (wt.%): C 51.4, O 45.9, Si 0.92, Ca 0.83, Mg 0.75, Na 0.23, and K 0.08. Similar values were obtained for fruit seed shells (wt.%): C 50.8, O 47.2, Si 0.57, Ca 0.49, Mg 0.64, Na 0.16, and K 0.12. The same elements were detected in the obtained activated carbons; however, their ratios changed markedly. In the final activated carbons, the elemental composition was (wt.%): C 89.87, O 7.82, Ca 1.49, Si 0.53, Mg 0.38, and Na 0.37. In some points, trace amounts of K, Fe, Al, Cl, and S were also observed.

The elemental composition of the spent adsorbents was as follows (wt.%): Uz-AD-1 (O 39.7-40.3; Al 35.2-37.1; Cl 15.8-17.7; Na 6.8-7.5) and Axsorb AA (O 23.5-50.3; Al 11.3-42.5; Cl 4.2-37.8; Na 2.9-22.03; Fe 0.1-5.4). The elemental composition of the prepared adsorbents and coagulants is summarized in Table 1, while their physicochemical characteristics are presented in Table 2.

3.2 Thermographic Analysis

By comparing differential thermal analysis (DTA) curves with thermogravimetric (TG) mass-loss curves for plant wastes (0.1 g) heated to 900 °C at 10 $°C \cdot min^{-1}$, and correlating these data with the yields of carbonizate and activated carbon, the temperature ranges corresponding to key thermal effects were determined experimentally.

Using peach seed shells as an example (Fig. 1, curve 1), decomposition of the main biomass occurred gradually over a broad temperature range and was characterized by overlapping exothermic effects with maxima at approximately 300, 339, and 639 °C. In the final pyrolysis stage, coking proceeded without distinct exothermic maxima. Endothermic effects with minima at about 44 and 122 °C were attributed to the removal of hygroscopic water at the initial stage, consistent with minor initial TG mass loss.

According to TG curves, the major mass loss (53-72%) occurred at 150-400 °C due to the decomposition of macromolecular components and formation of volatile products, including H_2O, CO, CO_2, CH_4, and C_2H_4 (chromatographic identification). At 400-640 °C, mass loss was 9-12%, with spatial rearrangement processes prevailing over further decomposition [26]. Above 650-700 °C, coking was accompanied by an additional gradual mass decrease of 5-8%. After carbonization at 700 °C (Fig. 1, curve 2), DTA curves of all studied wastes showed a single broad exothermic effect with a maximum near 290 °C. A second effect in the 600-700 °C region became more pronounced when carbonizates were subjected to alkaline modification. During steam activation, the total mass loss ranged from 50 to 65%.

Table 1: Elemental composition of adsorbents of various nature and coagulants obtained from waste.

Product Name	Element content; %										
	C	O	Ca	Mg	Na	Si	K	Fe	Al	Cl	S
AU-HS($NaHCO_3$)	8,63	51,2	18,1	5,64	2,05	6,97	1,74	0,42	--	-	0,03
AU-GP	6,34	29,5	33,3	11,3	1,06	7,37	-	-	-	6,13	0,42
AU-GP($NaHCO_3$)*	12,2	40,1	24,6	0,79	4,44	12,7	-	-	-	0,90	1,09
AU-GP ($NaHCO_3$)	13,6	46,9	17,1	5,23	6,7	4,77	-	-	-	-	-
OU-P	13,8	51,0	16,2	5,49	0,78	4,17	0,62	0,35	0,42	2,54	-
AU-P (NaOH)	11,3	51,8	14,2	5,03	8,16	6,49	-	-	-	-	-
OU-P (Na_2CO_3)	11,2	51,3	14,1	4,23	5,38	6,13	-	-	-	-	-
AU-P (HCl-NaOH)	4,65	54,5	14,3	2,34	8,98	7,31	-	-	-	-	-
OW-Ow	11,9	52,7	19,8	4,91	1,10	3,0	2,43	0,49	0,16	--	-
AU-A (H_{H2O}-NaOH)	6,44	52,5	15,5	2,74	10,1	7,6	--	-	-	-	-
OA-1	-	43,7	--	-	0,16	-	-	-	51,2	0.25	0,11
OA-1(NaOH)	-	43,3	--	-	5,12	-	-	-	46,2	0,08	0,07
K-1	-	38,2	--	-	0,8	-	-	-	16,7	25,1	14,7
K-2	-	27,1	--	-	0,5	--	-	1,5	12,5	23,4	9,85

*$NaHCO_3$The dried fraction of crushed guza pai was impregnated with NaHCO.

Thermal analysis of spent Uz-AD-1 (Fig. 2), with simultaneous analysis of released gases during heating in air, revealed a low-temperature endothermic effect near 55 °C, accompanied by ~5% mass loss due to desorption of physically adsorbed water, HCl, and C_4-C_5 hydrocarbons. An exothermic effect near 120 °C with a mass loss of 7.2% indicated oxidation of more strongly bound hydrocarbons. Subsequent thermal effects were associated with sublimation of $AlCl_3$ and dehydration of aluminum hydroxide phases (AlOOH/$Al(OH)_3$). Similar dehydration-related effects and phase transitions toward γ-alumina were observed for spent Axsorb AA. In thermograms of dried coagulants K-1 and K-2, the effect near 180 °C was weak due to overlap with endothermic removal of crystallization water from aluminum sulfate hydrates and related impurities.

3.3 X-ray Phase Analysis

XRD patterns of all investigated activated carbons showed two broad reflections: a moderate-intensity peak near $2\theta \approx 24°$ ($d \approx 0.3697$ nm) and a very weak peak near $2\theta \approx 43.5°$ ($d \approx 0.2674$ nm), indicating formation of turbostratic carbon during carbonization and subsequent thermal activation of plant wastes [34]. In several diffractograms, very weak but sharp peaks at $2\theta \approx 23.16, 24.86, 26.85, 29.48, 30.00, 30.84, 31.72, 35.08, 37.84$, and $50.6°$ were attributed to inorganic phases such as $CaSiO_3$, $CaCO_3$, $MgCO_3$, and Na_2CO_3.

According to diffraction patterns, the main phases in spent Uz-AD-1 and Axsorb AA were boehmite (AlOOH), γ-Al_2O_3 (broadened peaks), and crystalline NaCl (intense narrow peaks). Additional chloride hydrate phases (e.g., $AlCl_3 \cdot 6H_2O$) and traces of iron-containing phases were detected in Axsorb AA. The calcined OA-1 support exhibited broadened γ-Al_2O_3 peaks; after NaOH modification, additional narrow peaks appeared. The diffractogram of dried coagulant K-1 (Fig. 3) contained reflections of $AlCl_3$ hydrates and aluminum sulfate phases, including hydrated and anhydrous forms.

3.4 Functional Groups on the Surface of Activated Carbons

IR spectroscopy of raw plant wastes showed absorption bands typical of lignocellulosic materials: broad O-H stretching bands (≈3580-3560 cm^{-1}), C-H stretching bands of CH_2/CH_3 groups (≈2930-2820 cm^{-1}).

In unmodified carbon samples (e.g., AU-P, AU-HS), a broad intense band at 3500-3300 cm^{-1} was observed together with bands at ~2920 cm^{-1} (C-H stretching), ~1575 cm^{-1} (C=C stretching), and ~700 cm^{-1} (C-H deformation). In AU-A, additional bands attributable to phenolic hydroxyl groups and possible hydrated inorganic impurities were observed. After modification with sodium carbonate (e.g., AU-A (Na_2CO_3)), the strong broad band near 3300 cm^{-1} reflected contributions from hydroxyl-containing groups (carboxyl/phenolic), while the C=O stretching band near 1660 cm^{-1} and carboxylate bands near 1400 and 1580 cm^{-1} indicated enhanced carboxylate structures. Bands at 865, 753, and 663 cm^{-1} were assigned to out-of-plane C-H deformation vibrations in polynuclear aromatic structures. The corresponding FTIR spectra are presented in Figure 4.

Table 2: Physical and chemical characteristics of adsorbents.

Indicators	AY-HY	AY-HY($NaHCO_3$)	AY-GP	AY-GP($NaHCO_3$)	AU-P	AU-P (NaOH)	AU-P (Na_2CO_3)	AU-P (HCl-NaOH)	AY-	AY-A (H_2O-NaOH)	*OA-1*	*OA-1 (NaOH)*	*OA-1 ToOH)*
Bulk density, g/DM³	425	429	428	41 5	444	450	405	402	432	398	*650*	*673*	*684*
Strength: abrasion, % *Kg granule*	78	79	74	65,7	87	85	82	86	89	87	*2,11*	*2,08*	*2,04*
Dynamic activity of benzene, g/DM³	120	127	105	103	118	121	83	125	107	125	*Virtually no*		
Activity on iodine, %	48	51,2	43,2	42,8	51	53	does Not determine						
the Ash content, %	5,64	Of 5.82	8,0	2,9	5.0	5.0	3,4	1,8	4,8	2,3	-	-	-
Specific surface area, m²/g	695	783	430	525	718	820	730	835	652	754	*238*	*147*	*128*
Total pore volume, cm³/g	0,90	0,97	0,87	0,79	0,93	0,98	0,84	0,91	0,53	0,86	*0,55*	*0,48*	*0,41*
the Volume of mesopores cm³/g	0,12	0,23	0,11	0,10	0,09	0,20	0,25	0,24	0,17	0,31	*0,22*	*0,20*	*0,19*
the Volume of micropores, cm³/g	0,48	0,44	0,40	0,32	0,36	0,38	0,18	0,47	0,34	0,29	*0,21*	*0,12*	*0,11*
Adsorption of methylene blue; mg/g	152	180	111	118	173	178	145	186	122	154	*18*	*5*	*4*

Quantification of surface functional groups by the Boehm method [30] was supported by potentiometric titration with selective reagents, confirming the diversity of surface sites (e.g., H^+, -COOH, phenolic -OH, alcoholic -OH). For AU-A, the concentrations (mmol·g⁻¹) were: carboxylic 0.004, phenolic 0.017, alcoholic 0.080, and total surface acidity 0.101. Surface basicity for AU-A was 0.22 mmol·g⁻¹, remaining nearly unchanged after alkaline modification of raw materials but increasing to 0.29-0.42 mmol·g⁻¹ after carbonate modification.

3.5 Adsorption Performance

Pharmaceutical production involves periodic multi-stage operations, which leads to a broad spectrum of drugs, precursors, and suspended solids in effluents (e.g., during equipment washing and room cleaning). Wastewater from injection-solution production (COD 500-2000 mg $O_2 \cdot L^{-1}$) was simulated by dissolving the contents of a defined number of pharmaceutical ampoules in 5 L of distilled water. The experimentally determined COD values (mg $O_2 \cdot L^{-1}$) for individual solutions were: (1) cyanocobalamin (427), (2) rifamycin phosphate (986), (3) lincomycin hydrochloride (1739), (4) methylene blue (790), (5) lidocaine (856), (6) dibazole (789), and (7) pyridoxine hydrochloride (302). Mixing equal volumes of solutions (1)-(7) produced model mixture "A" with COD 841 mg $O_2 \cdot L^{-1}$.

Model solutions for oral preparations (8)-(16) were prepared by dissolving powders/capsule contents/crushed tablets in tap water (including poorly soluble components). The following COD values (mg $O_2 \cdot L^{-1}$) were obtained: (8) erythromycin phosphate (792), (9) ceftriaxone (1010), (10) doxycycline hydrochloride (572), (11) chlortetracycline (1184), (12) cefuroxime (1443), (13) diphenhydramine (190), (14) ibuprofen (1086), (15) ascorbic acid (283), and (16) paracetamol (447). Mixing equal volumes of solutions (8)-(16) yielded model mixture "B" (COD 778 mg $O_2 \cdot L^{-1}$), characterized by high turbidity and representative of antibiotic-production wastewater and domestic wastewater containing pharmaceuticals.

Changes in COD during treatment with AU-P (HCl-NaOH) are shown in Figure 5 (curves A-3 and B-1). Pretreatment with coagulant K-1 followed by settling reduced COD as shown by curves A-1 and B-2 (Fig. 5). The effect of a two-layer bed of AU-A (H_2O-NaOH) and OA-1 (NaOH) was also evaluated (curve A-2), including a variant using coagulant K-2 (curve A-4). Gas-phase adsorption of volatile reagents commonly used in pharmaceutical production was tested for AU-P (HCl-NaOH), AU-A (H_2O-NaOH), AU-HS ($NaHCO_3$), and OA-1 (NaOH); breakthrough curves are presented in Figure 6.

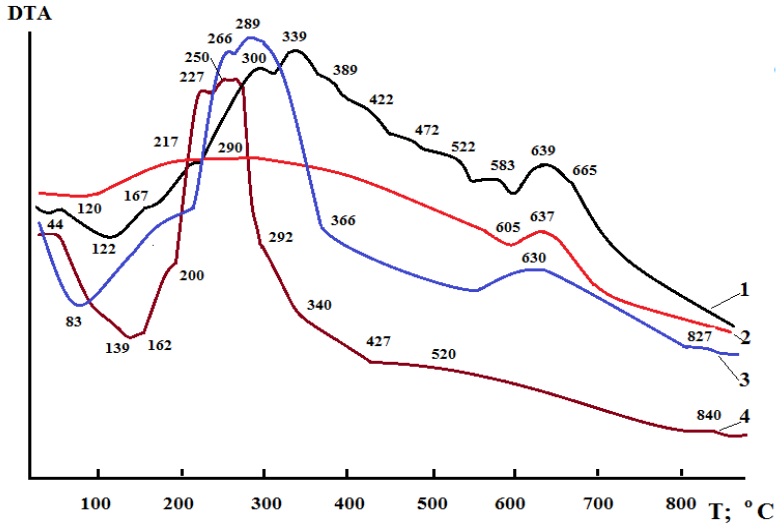

Figure 1: Thermograms of peach seed shells modified with sodium carbonate (in nitrogen current) - 1; AU carbonizate-P (Na_2CO_3) (in nitrogen current - - 2; 3-reactivation of AU-P (HCl-NaOH) used in wastewater treatment A, 4-reactivation of the AC-P (HCl-NaOH) used in the treatment of gas emissions.

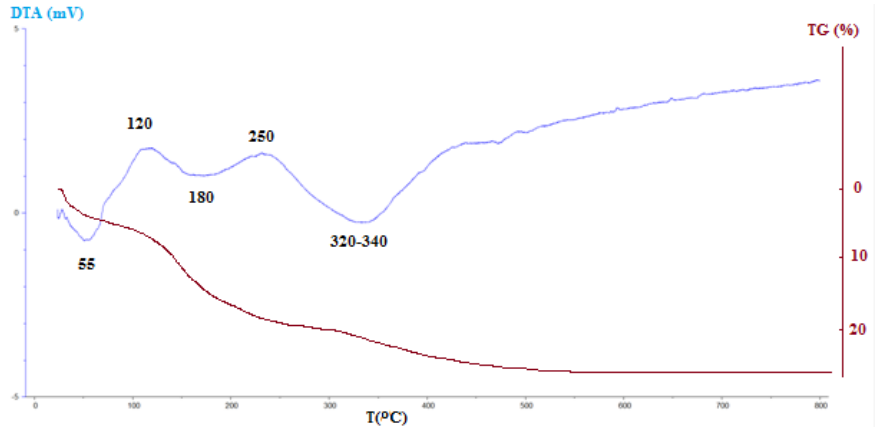

Figure 2: Thermogram of spent adsorbent Uz-AD-1.

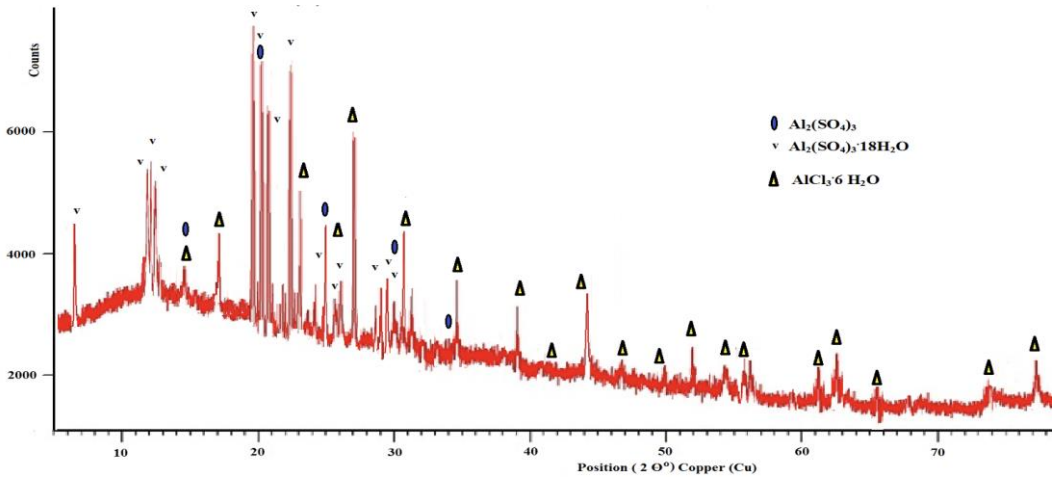

Figure 3: Diffractogram of dried coagulant K-1.

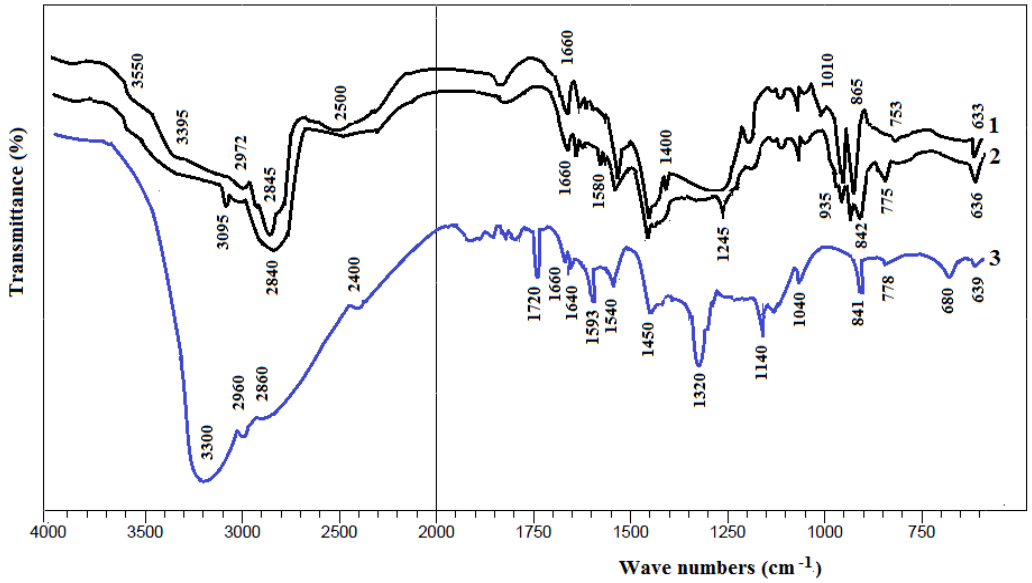

Figure 4: IR spectra of activated carbons. 1 - AU-A (Na_2CO_3); 2 - AU-A (Na_2CO_3) after trichloroethylene adsorption; 3 - AU-A (Na_2CO_3) after purification of the model wastewater solution - "A".

4 DISCUSSION

Comparison of activated carbon yields with thermographic analysis data demonstrated that modification of carbonizates with alkali metal compounds slowed the burnout process during steam activation. This effect promoted more complete removal of liquid activation products and facilitated pore opening, resulting in the formation of wide slit-like mesopores. The positive influence of alkaline modification was further enhanced by sequential treatment of the initial plant shells with hot HCl solution followed by water washing to pH 7, or alternatively by boiling in water and drying to constant mass at 110-120 °C.

Textural characteristics obtained by mercury porosimetry were consistent with the results of porous structure evaluation using molecular probe substances with different critical molecular diameters (H_2O, 0.27 nm; CH_3OH, 0.40 nm; phenol, 0.63 nm; CCl_4, 0.69 nm) as well as larger dye molecules (methylene blue, 0.47 × 0.84 × 1.60 nm; crystal violet, 1.42 × 1.23 × 0.62 nm; bromothymol blue, 1.22 × 0.98 × 1.02 nm). These data indicated the predominance of bottle-shaped pores with diameters of approximately 0.5 nm in the activated carbons (Table 2). As shown in Table 2, adsorption capacities determined using iodine and methylene blue tests correlated more strongly with mesopore volume.

Reduction in ash content for AU-P (HCl-NaOH) and AU-A (H_2O-NaOH), confirmed by XRD through the absence of Ca and Mg silicate and carbonate phases, resulted in increased porosity and enhanced adsorption of methylene blue, a marker of low-molecular-weight toxic compounds. Although the specific surface area of the prepared carbons was lower than that of commercial F-400 carbon (977 $m^2 \cdot g^{-1}$) [29], Fluka carbon (880 $m^2 \cdot g^{-1}$) [34], and apple-peel-based carbon (854 $m^2 \cdot g^{-1}$) [24], the maximum methylene blue adsorption capacity of AU-P (HCl-NaOH) reached 186 $mg \cdot g^{-1}$. This value exceeded those reported for activated carbons derived from brown coal (178 $mg \cdot g^{-1}$) [30], rice husk (60.1 $mg \cdot g^{-1}$), and oil palm wood (90.9 $mg \cdot g^{-1}$), while remaining lower than values reported for bamboo-based (454.2 $mg \cdot g^{-1}$) and flamboyant pod-based carbons (874.68 $mg \cdot g^{-1}$) [25].

The IR spectra of activated carbons obtained from plant-based waste were generally consistent with literature data [24], [35]. Bands corresponding to phenolic and carboxyl functional groups were similar to those reported for apple-peel-derived activated carbon produced using microwave irradiation [24]. The spectral patterns in Figure 4 were comparable to those of commercial Loba Chemie activated carbon [10], although the intense C-N stretching band was absent. Reported FTIR spectra of F-400 carbon [29] showed characteristic bands at 1240, 1610, and 1750 cm^{-1}; however, attribution of these bands remains ambiguous due to overlapping contributions from ether, epoxide, phenolic, and carbonyl structures. The absence of lactone bands in the present samples may be explained by their thermal instability during carbonization.

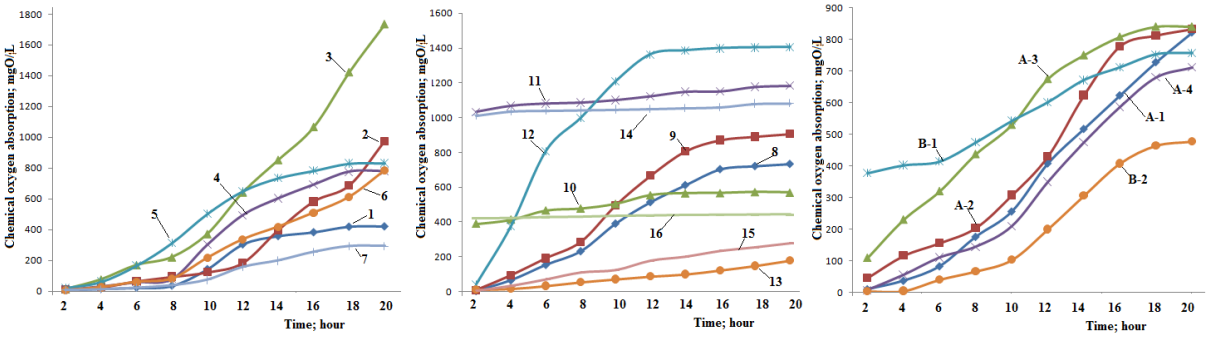

(a) (b) (c)

Figure 5: Changes in wastewater chemical oxygen demand (COD) during adsorption on activated carbon under different treatment conditions.

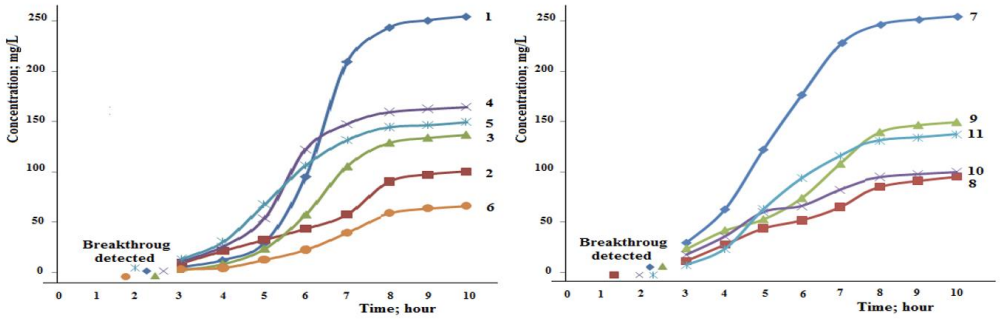

(a) (b)

Figure 6: Breakthrough curves for the adsorption of volatile organic compounds on activated carbons obtained from plant waste: a) AU-P (HCl-NaOH), b) comparative curves for AU-A (H_2O-NaOH), AU-HS ($NaHCO_3$), and OA-1 (NaOH).

Figure 5 illustrates the variation in chemical oxygen demand (COD) during wastewater treatment under different experimental conditions. Figure 5a presents the COD reduction for wastewater containing individual pharmaceutical compounds (Nos. 1–16) during filtration through the AU-P (HCl–NaOH) adsorbent. Figure 5b compares the treatment of model mixture A (injectable pharmaceutical solutions) before and after pre-coagulation, demonstrating the positive effect of coagulation on adsorption efficiency. Figure 5c shows the corresponding results for model mixture B (solid pharmaceutical powders) before and after pre-coagulation, together with the performance of a double-layer adsorbent bed consisting of AU-A (H_2O–NaOH) and OA-1 (NaOH) for mixture A.

In contrast to microporous activated carbon derived from natural coal [29], which contains higher concentrations of surface functional groups, the synthesized adsorbents demonstrated superior removal efficiency for water-soluble antibiotics, anesthetics, and methylene blue in high-COD model wastewater. Among the investigated materials, AU-P (HCl-NaOH) exhibited the highest adsorption efficiency, which can be attributed to its larger mesopore volume. The adsorption performance of AU-P (Na_2CO_3), characterized by a lower mesopore volume, was approximately 12% lower.

Analysis of the IR spectra of spent AU-P (Na_2CO_3) revealed the appearance of broad O-H/N-H stretching bands (approximately 3300 cm^{-1}) together with absorption bands corresponding to saturated hydrocarbons, cyclic compounds, and carbonyl groups, indicating adsorption of organic contaminants. Combined interpretation of the IR spectra and COD measurements showed that during the first 2 h of dynamic operation an 80 cm bed of AU-P (HCl-NaOH) achieved a COD removal efficiency of 88.1%.

Figure 5 also demonstrates the positive effect of coagulation pretreatment. The application of coagulants K-1 and K-2 reduced the methylene blue concentration from 25 mg L^{-1} to 6.23 and 5.92 mg L^{-1}, respectively, which is comparable to the performance of commercial aluminum sulfate. In addition, COD of model mixtures A and B

decreased by 13% and 38%, respectively, while turbidity was reduced by up to 75%.

Gas-phase adsorption studies (Fig. 6) showed that AU-P (HCl-NaOH) effectively reduced concentrations of volatile toxic compounds formed during vitamin B_6 production to below maximum permissible concentrations within 3-5 h. Regenerated activated carbons retained 93-94% of their adsorption capacity. AU-A (H_2O-NaOH) demonstrated superior adsorption of larger molecules such as trichloroethylene, while OA-1 (NaOH) effectively removed inorganic chlorine compounds. These results confirm the applicability of waste-derived activated carbons and alumina-based adsorbents for integrated treatment of pharmaceutical wastewater and gas emissions.

5 CONCLUSIONS

An alkaline modification technology was developed for the production of aluminum oxide and carbon adsorbents derived from wastes of the cotton and canning industries. The obtained materials exhibited a specific surface area of 754-835 $m^2 \cdot g^{-1}$ and a methylene blue adsorption capacity of 154-186 $mg \cdot g^{-1}$. Using model wastewater and gas emission systems, it was demonstrated that up to 95-98% of toxic compounds can be removed under optimal treatment conditions and appropriate adsorbent bed thickness.

The proposed approach enables effective reduction of environmental risks associated with the release of antibiotics and other pharmaceutical substances into natural ecosystems via industrial, domestic, and agricultural waste streams. The utilization of industrial waste as a raw material, in line with circular economy principles, represents a sustainable and resource-efficient alternative to conventional adsorbent production. Furthermore, adsorption-based treatment of industrial effluents contributes to mitigating the conflict between economic development and environmental protection, supporting compliance with environmental regulations and long-term sustainability goals.

REFERENCES

[1] J. Gao, J. Huang, W. Chen, et al., "Fate and removal of typical pharmaceutical and personal care products in a wastewater treatment plant from Beijing: A mass balance study," Front. Environ. Sci. Eng., vol. 10, pp. 491-501, 2016.

[2] A. G. Parvatker, J. D. Sherman, C. Philip, A. Paul, J. B. Zimmerman, and M. J. Eckelman, "Cradle-to-gate greenhouse gas emissions for twenty anesthetic active pharmaceutical ingredients based on process scale-up and process design calculations," ACS Sustain. Chem. Eng., vol. 7, pp. 6580-6591, 2019, [Online]. Available: https://doi.org/10.1021/acssuschemeng.8b05473.

[3] L. F. Angeles, R. A. Mullen, I. J. Huang, C. Wilson, W. Khunjar, H. I. Sirotkin, and A. E. Elroy, "Assessing pharmaceutical removal and reduction in toxicity provided by advanced wastewater treatment systems," Environ. Sci.: Water Res. Technol., vol. 6, pp. 62-77, 2020.

[4] H. T. Elbalkiny, A. M. Yehia, S. M. Riad, and Y. S. Elsaharty, "Removal and tracing of cephalosporins in industrial wastewater by SPE-HPLC: Optimization of adsorption kinetics on mesoporous silica nanoparticles," J. Anal. Sci. Technol., vol. 10, pp. 1-10, 2019.

[5] S. Aissaoui, H. Ouled-Haddar, M. Sifour, et al., "Biological removal of mixed pharmaceuticals using a bacterial consortium," Iran. J. Biotechnol., vol. 15, pp. 136-142, 2017.

[6] A. J. Ebele, M. E. Abdallah, and S. Harrad, "Pharmaceuticals and personal care products (PPCPs) in the freshwater aquatic environment," Emerg. Contam., vol. 3, pp. 1-16, 2017.

[7] S. Gulomov, D. Turdieva, N. Isaeva, D. Z. Narzullaev, and K. K. Shadmanov, "Catalytic neutralization of gas emissions in pharmaceutical manufacturing," E3S Web Conf., vol. 411, Art. no. 02024, 2023.

[8] H. Kaur, A. Bansiwal, G. Hippargi, and G. R. Pophali, "Effect of hydrophobicity of pharmaceuticals and personal care products on adsorption by activated carbon," Environ. Sci. Pollut. Res., vol. 25, pp. 20473-20485, 2018.

[9] N. M. Mahmoodi, M. Taghizadeh, and A. Taghizadeh, "Mesoporous activated carbons from agricultural bio-wastes with high adsorption capacity," J. Mol. Liq., vol. 269, pp. 217-228, 2018.

[10] E. Mourid, M. Lakraimi, E. E. Khattabi, L. Benaziz, and M. Berraho, "Removal of textile dye Acid Green 1 from wastewater by activated carbon," J. Mater. Environ. Sci., vol. 8, pp. 3121-3130, 2017.

[11] H. Sukmana, N. Bellahsen, F. Pantoja, and C. Hodur, "Adsorption and coagulation in wastewater treatment: A review," Prog. Agric. Eng. Sci., vol. 17, pp. 49-68, 2021, [Online]. Available: https://doi.org/10.1556/446.2021.00029.

[12] E. V. Korchagina, M. Y. Piskunova, A. V. Ryzhenkova, and A. V. Nistratov, "Approaches to removing persistent organic dyes from aqueous solutions," Chem. Technol. Fuels Oils, vol. 34, pp. 59-61, 2018.

[13] M. S. Safwat, Y. M. Nouran, N. A. Mohamed, and E. Abdelsalam, "Adsorption of phenol onto aluminum oxide nanoparticles," Adsorpt. Sci. Technol., vol. 2022, Art. no. 1924117, 2022.

[14] T. Crovella and A. Paiano, "Assessing the sustainability of photodegradation and photocatalysis for wastewater reuse," Water, vol. 15, p. 2758, 2023, [Online]. Available: https://doi.org/10.3390/w15152758.

[15] J. Cai, M. Zhou, Y. Pan, and X. Du, "Extremely efficient electrochemical degradation of organic pollutants on Blue-TiO_2 nanotube anodes," Appl. Catal. B Environ., vol. 257, Art. no. 117902, 2019, [Online]. Available: https://doi.org/10.1016/j.apcatb.2019.117902.

[16] S. Yuan, H. Hu, H. Huang, Z. Chen, J. Chen, M. Zhang, K. Li, T. Zhou, and R. Lv, "Reaction pathways of chlorobenzene oxidation in electrochemical-persulfate systems," J. Clean. Prod., vol. 420, Art. no. 138336, 2023.

[17] N. Chen, D. Lee, H. Kang, and D. Cha, "Catalytic persulfate activation for oxidation of organic pollutants: A critical review," J. Environ. Chem. Eng., vol. 10, Art. no. 107654, 2022, [Online]. Available: https://doi.org/10.1016/j.jece.2022.107654.

[18] Q. Gao, J. Ding, G. Zhao, Q. Zhao, L. Li, X. Zhao, L. Bu, S. Zhou, and S. Qiu, "Synergistic effects of sunlight and electrooxidation on persulfate activation," Chem. Eng. J., vol. 428, Art. no. 135318, 2022, [Online]. Available: https://doi.org/10.1016/j.cej.2022.135318.

[19] C. Dong, W. Fang, Q. Yi, and J. Zhang, "Reactive oxygen species in advanced oxidation processes: A comprehensive review," Chemosphere, vol. 308, Art. no. 136205, 2022, [Online]. Available: https://doi.org/10.1016/j.chemosphere.2022.136205.

[20] A. Fayyaz, C. M. Park, Y. Yoon, and K. Talukdar, "Catalytic oxidation of naproxen in persulfate systems," Chem. Eng. J., vol. 407, Art. no. 127842, 2020, [Online]. Available: https://doi.org/10.1016/j.cej.2020.127842.

[21] E. Besedova, D. Bobok, S. Bafrncova, and P. Steltenpohl, "Modelling of gas-phase adsorption on activated carbon," Chem. Pap., vol. 58, pp. 391-396, 2004.

[22] M. W. Ashraf, N. Abulibdeh, and A. Salam, "Adsorption of chrysoidine dye using activated sawdust," Int. J. Chem. Eng., vol. 2019, Art. no. 9728156, 2019.

[23] F. G. de Oliveira, C. R. de Andrade, M. A. G. Trindade, H. M. C. de Carvalho, and T. C. de Carvalho, "Thermogravimetric and spectroscopic study of activated carbon from babassu biomass," Quim. Nova, vol. 40, pp. 284-292, 2017, [Online]. Available: https://doi.org/10.21577/0100-4042.20160191.

[24] R. H. Hesas, A. Arami-Niya, W. M. A. W. Daud, and J. N. Sahu, "Preparation of activated carbon from apple waste," BioResources, vol. 8, pp. 2950-2966, 2013.

[25] A. M. M. Vargas, A. L. Cazetta, M. H. Kunita, T. L. Silva, and V. C. Almeida, "Adsorption of methylene blue on activated carbon from flamboyant pods," Chem. Eng. J., vol. 168, pp. 722-730, 2011, [Online]. Available: https://doi.org/10.1016/j.cej.2011.01.067.

[26] M. G. Ismailova, A. R. Gutnikova, and P. L. Ismailova, "Enterosorbent AU-K and its pharmacological activity," Bull. Pharm., vol. 2, pp. 1-6, 2010.

[27] S. B. Dzhalalova, T. B. Molodozhenyuk, M. P. Yunusov, S. N. Namazbaev, and V. V. Lavoshnikov, "Activated carbons from cotton lignin for water conditioning," Chem. Technol. Fuels Oils, vol. 41, pp. 129-133, 2005.

[28] M. P. Yunusov, K. A. Nasullaev, S. T. Gulomov, N. F. Isaeva, B. D. Mustafaev, B. B. Rakhimjanov, and R. G. Khodjiev, "Experimental sorbents for chloride compound removal," Chem. Probl., vol. 18, pp. 366-375, 2020.

[29] B. Li, "Characterization of pore structure and surface chemistry of activated carbons," in Fourier Transform-Materials Analysis, S. Salih, Ed. Rijeka, Croatia: InTech, 2012, pp. 165-190.

[30] K. Mahmoudi, N. Hamdi, and E. Srasra, "Adsorption of methylene blue on activated carbon from lignite," Surf. Eng. Appl. Electrochem., vol. 51, pp. 427-433, 2015, [Online]. Available: https://doi.org/10.3103/S1068375515050105.

[31] R. M. Silverstein, G. C. Bassler, and T. C. Morrill, Spectrometric Identification of Organic Compounds. New York, NY, USA: Wiley, 1991.

[32] B. N. Tarasevich, IR Spectra of the Main Classes of Organic Compounds. Moscow, Russia, 2012.

[33] E. Pretsch, P. Bühlmann, and M. Badertscher, Structure Determination of Organic Compounds, 4th ed. Berlin, Germany: Springer, 2009.

[34] M. Ilić, F. H. Haegel, A. Lolić, Z. Nedić, T. Tosti, I. S. Ignjatović, et al., "Surface functional groups and degree of carbonization of chars," PLoS ONE, vol. 17, Art. no. e0277365, 2022.

[35] X. Teng, J. Li, Z. Wang, Z. Wei, C. Chen, K. Du, C. Zhao, and G. Yang, "Performance and mechanism of methylene blue degradation by electrochemical processes," RSC Adv., vol. 10, pp. 24712-24720, 2020, [Online]. Available: https://doi.org/10.1039/D0RA03963B.